

# Leveraging a Small Dataset to Predict Nonlinear Global Loads

Kyle E. Marlantes\* and Kevin J. Maki

## ABSTRACT

*In this work, a hybrid machine learning method, which uses ML strategies to model high-order force components within a low-order equation of motion, is considered in the context of the global wave-induced loads of a ship in irregular waves. It is shown that the method can make predictions in a range of wave conditions even when the training data set only includes a single seaway. The proposed method offers a data-leveraging technique which may be useful in the design space, where a small data set derived from a high-fidelity source can be leveraged to make similar fidelity predictions in a larger number of wave conditions.*

## KEY WORDS

Wave-induced; global loads; shear forces; bending moments; hybrid machine learning

## INTRODUCTION

Global wave-induced loads are an important consideration in the design of ship structures. Often, shear forces and bending moments are estimated using rules-based distributions or simplified quasi-static methods (Payer and Schellin, 2013). Though practical for early-stage design, research has shown that real-world measurements can exceed rules-based predictions (Andersen and Jensen, 2014). In many cases, linear frequency-domain hydrodynamic tools such as strip theory are used (Payer and Schellin, 2013). However, it is well-known that such low-fidelity methods can underpredict the maximum bending moment (Wu and Hermundstad, 2002), (Rajendran et al., 2016), (Gaspar et al., 2016), sometimes by as much as 32% when considering long-term responses (Parunov et al., 2022a), and compensating with large safety margins may lead to an over-designed structure (Parunov et al., 2022b).

Nonlinear global loads are predominantly a second-order effect (Juncher and Terndrup, 1979), (Marlantes and Taravella, 2019) and strongly related to the body-nonlinear hydrodynamic forces, so it is necessary to use nonlinear numerical models. However, high-fidelity computational hydrodynamic tools, such as Reynolds Averaged Navier-Stokes (RANS) CFD methods or nonlinear potential flow methods, especially if coupled to a structural solver, suffer from a high computational cost, making it impractical to evaluate a large number of wave conditions (Hirdaris et al., 2014), (Temarel et al., 2016). As a result, body-nonlinear methods, which model the Froude-Krylov and hydrostatic restoring forces nonlinearly, are popular tools, as the nonlinearity from these forces capture much of the difference between hogging and sagging bending moments (Guedes Soares, 1991), which is especially evident in ships with large flare (Rajendran et al., 2016). One promising approach for high-fidelity methods is to use design waves, such as the Design Loads Generator proposed in Alford (2008) and

---

Department of Naval Architecture and Marine Engineering, University of Michigan, Ann Arbor, USA

\* Corresponding Author: [kylemarl@umich.edu](mailto:kylemarl@umich.edu)

Submitted: 22 February 2024, Revised: 29 April 2024, Accepted: 1 May 2024, Published: 21 May 2024

©2024 published by TU Delft OPEN Publishing on behalf of the authors. This work is licensed under CC-BY-4.0.

Conference paper, DOI: <https://doi.org/10.59490/imdc.2024.873>

e-ISSN: 3050-4864

Alford et al. (2011) or the Critical Wave Groups method in Anastopoulos and Spyrou (2016), which greatly reduce the simulation time required. The role of simulators in design is enticing, but without the ability to identify “edges” in the design space, their usefulness is reduced (Schellin et al., 2015). Developing new computational methods which preserve nonlinearity, but are inexpensive to evaluate in a large number of wave conditions, is important to advancing simulation-based design (Hirdaris et al., 2014).

In recent years, machine learning (ML) methods have been explored to reduce the computational cost of predictions, but the accuracy of most ML methods is reduced when making predictions in wave conditions which differ from the original training dataset, and most data-only methods require a large amount of training data (Portillo Juan and Negro Valdecantos, 2022). Hybrid machine learning methods, which combine physics with ML techniques, have been shown to reduce the training data requirements (Willard et al., 2020). However, few examples of hybrid machine learning methods applied to global wave-induced loads are found in the literature. Several examples of data-only methods, such as the work of Moreira and Soares (2020), Hou et al. (2024), and Kwon et al. (2022) have been given, and a recent, and novel, approach in Wang and Ti (2024) which considers the wave-induced loads on bridge structures with arbitrary shapes. Several studies also take a probabilistic approach, such as the Bayesian models described in Zhu and Collette (2017). However, most studies focus on structural health monitoring in real-time, fatigue monitoring, or structural event detection. Moreover, most of these studies considered in-situ applications where data is plentiful, which often precludes their use in a design or analysis scenario, especially for unusual designs.

In this work, the hybrid machine learning method of Marlantes and Maki (2022) is considered in the context of the global wave-induced loads problem. The method relates a high-fidelity and low-fidelity model by a force correction that is modeled using an artificial neural network. To illustrate, Eq. (1) is the high-fidelity model, indicated by the superscript ( $h$ ), and the solution to this differential equation is the high-fidelity state  $\ddot{z}^{(h)}$ . This model might be a RANS-CFD simulation or a fully-nonlinear three-dimensional panel method, but in general, the high-fidelity model is assumed to be both more accurate and significantly more expensive to evaluate. Eq. (2) is the low-fidelity model—a model that is inexpensive to solve but lacks accuracy—indicated by superscript ( $l$ ), where the solution to the equation is the low-fidelity state  $\ddot{z}^{(l)}$ .

$$m\ddot{z}^{(h)} = f^{(h)} \quad (1)$$

$$m\ddot{z}^{(l)} = f^{(l)} \quad (2)$$

Adding and subtracting the low-fidelity force model  $f^{(l)}$  from Eq. (2) from the right-hand-side of Eq. (1) results in a force correction term  $\delta$ , as shown by Eq. (4).

$$m\ddot{z}^{(h)} = f^{(l)} + f^{(h)} - f^{(l)} \quad (3)$$

$$m\ddot{z}^{(h)} = f^{(l)} + \delta \quad (4)$$

An analytical model for  $\delta$  may not be available, so it is modeled using an artificial neural network, which introduces an error  $\epsilon = \delta - \delta^*$ , where  $\delta^*$  is the approximate force correction obtained by the trained model. Considering this error, Eq. (4) becomes Eq. (5). A solution to Eq. (5) will yield an approximate high-fidelity state  $\ddot{z}^*$  which will approach  $\ddot{z}^{(h)}$  as  $\epsilon \rightarrow 0$ .

$$m\ddot{z}^* = f^{(l)} + \delta^* \quad (5)$$

Both recurrent neural networks like Long Short-Term Memory (LSTM) and simpler feed-forward densely-connected multi-layer networks have been used to model  $\delta$ , but it is found in Marlantes et al. (2023) that relatively small, simple networks are sufficient for ship hydrodynamics problems, with the added benefit that they are inexpensive to train and evaluate. The

primary consideration when designing the network is to accommodate numerical integration of Eq. (5). To this end,  $\delta$  is modeled as a function of  $k$ -length discrete sequences of prior state  $\{z\}_{n-k-1}^n$ ,  $\{\dot{z}\}_{n-k-1}^n$ ,  $\{\ddot{z}\}_{n-k-1}^n$  and the wave elevation  $\{\eta\}_{n-k-1}^n$ , where the current time is  $t^n$ . Therefore, the state and wave elevation comprise the input features of the neural network and the output is simply  $\delta^{*,n+1}$ .

In this paper, Eq. (5) is extended to the global loads problem by means of classical rigid beam theory. Of specific interest is how well the method performs in wave conditions which differ from the training dataset, and the role that the low-fidelity forcing model  $f^{(l)}$  plays in this behavior. This property, known as generalizability, is critical to using data-driven simulation methods in a design scenario, where limited data is the norm. The ability to train a model of  $\delta$  on a small, initial dataset, and then make predictions of wave-induced loads at similar fidelity in many additional wave conditions could provide considerable insight into the performance of a design.

## THEORY

The classical model of global shear forces and bending moments assumes the hull behaves as a single rigid beam, as shown in Figure 1. While this model is greatly simplified, it will be used as the basis for this work as it encompasses the essential physics. The total length of the beam  $L$  is taken as the principle length of the vessel under consideration. We restrict the hull girder to move only in the vertical direction,  $z$ , such as in the heaving motion of a vessel in a seaway, reducing the problem to a single degree-of-freedom (DOF) system. As a consequence, any effect pitch motion may have on the nonlinear shear and bending moment is not considered. This simplifies the formulation of the hydrodynamic forces as they will depend only on heave motion and wave elevation, and will not have any coupling into rotation, which may alter the amplitude, frequency, or phase of the response.

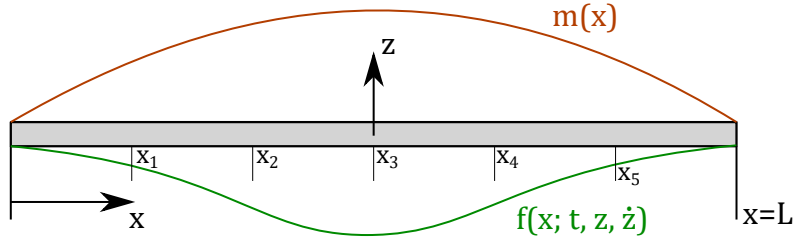


**Figure 1: Hull girder as a rigid beam. The physical mass distribution  $m(x)$  is time-invariant. The hydrodynamic force distribution  $f(x; t, z, \dot{z})$  is shown at an instant in time  $t$ .**

The dynamics of the rigid hull girder shown in Figure 1 follow Eq. (6), where the total physical mass  $M$  is the integral of the longitudinal mass distribution  $m(x)$  and is assumed to be time-invariant. The total hydrodynamic force  $F(t; z, \dot{z})$  varies with time  $t$  and is nonlinear with respect to the state variables  $z, \dot{z}$  and is found by integrating the sectional hydrodynamic forces  $f(x; t, z, \dot{z})$  over the length of the hull. Note that because the beam is rigid and moving only in heave, the vertical acceleration  $\ddot{z}$  is pulled out of the integral on the left-hand-side of Eq. (7).

$$M\ddot{z} = F(t, z, \dot{z}) \quad (6)$$

$$\ddot{z} \int_0^L m(x) dx = \int_0^L f(x; t, z, \dot{z}) dx \quad (7)$$

The total force  $F(t; z, \dot{z})$  is nonlinear, high-fidelity, and assumed to be exact. Following the method outlined in the introduction, the high-fidelity total force  $F(t, z, \dot{z})$  can be expressed in terms of a force correction  $\Delta(t, z, \dot{z})$  to some inexpensive and low-order forcing model  $F^{(l)}(t, z, \dot{z})$ , given by Eq. (8). Similarly, the low-order total force  $F^{(l)}$  and force correction  $\Delta$  are the integral of their sectional counterparts  $f^{(l)}$  and  $\delta$ , respectively.

$$F(t, z, \dot{z}) = F^{(l)}(t, z, \dot{z}) + \Delta(t, z, \dot{z}) \quad (8)$$

$$= \int_0^L f^{(l)}(x; t, z, \dot{z}) dx + \int_0^L \delta(x; t, z, \dot{z}) dx \quad (9)$$

The instantaneous vertical shear force  $V$  at time  $t$  at a section  $x = s$  balances the difference between the inertial forces  $I$  and hydrodynamic forces  $F$  acting on the hull girder up to  $s$ , as given by Eq. (10). The internal bending moment is found by a nearly identical process after including the lever-arm  $(x - s)$  in the integrand, so for brevity it will not be presented here. We extend the same force-correction approach from Eq. (8) to the vertical shear force and bending moment. The resulting expression for shear is given by Eq. (12).

$$V(s; t) = I(s; t) - F(s; t, z, \dot{z}) \quad (10)$$

$$= \ddot{z} \int_0^s m(x) dx - \int_0^s f(x; t, z, \dot{z}) dx \quad (11)$$

$$= \ddot{z} \int_0^s m(x) dx - \int_0^s [f^{(l)}(x; t, z, \dot{z}) + \delta(x; t, z, \dot{z})] dx \quad (12)$$

The sectional low-fidelity forcing model  $f^{(l)}(x; t, z, \dot{z})$  and force correction  $\delta(x; t, z, \dot{z})$  in Eq. (12) are the same terms as in Eq. (9). Therefore, we restrict our focus to the sectional forces at  $x = s$ , and express the dynamics of a section as Eq. (14), which is simply the two-dimensional version of Eq. (6). If the sectional forces  $f^{(l)}$  and  $\delta$  are modeled, the shear force and bending moment will follow.

$$m(s)\ddot{z}_s = f(s; t, z_s, \dot{z}_s) \quad (13)$$

$$= f^{(l)}(s; t, z_s, \dot{z}_s) + \delta(s; t, z_s, \dot{z}_s) \quad (14)$$

While a solution of Eq. (14) will yield a  $\ddot{z}_s$  that is indeed different than  $\ddot{z}$ , due to the rigid body assumption, it differs by only a constant factor equal to  $L$ . Therefore, a solution to Eq. (14) captures the same underlying dynamics of the global problem and an investigation of Eq. (14) will allow us to make conclusions about Eq. (10). In the remainder of this work, we will focus primarily on Eq. (14), as it is the fundamental building block of the global loads problem.

## Duffing Equation

To investigate the choice of  $f^{(l)}$  on the performance of the method, a forced Duffing equation is used as a theoretical model of the sectional hydrodynamic force  $f(s; t, z_s, \dot{z}_s)$ , as it captures the salient features of the nonlinear hydrodynamics problem of a ship in waves. The Duffing equation model is given by Eq. (15), where  $c_1$  and  $c_3$  are the linear and cubic hydrostatic restoring coefficients,  $b_1$  and  $b_2$  are the linear and quadratic hydrodynamic damping coefficients, and the wave excitation forcing due to irregular waves is expressed as a summation of harmonic wave components. The wave excitation is made nonlinear by including the state  $z_s$  in the amplitude, modified by a coefficient  $\alpha$ .

$$m(s)\ddot{z}_s = \sum_i (\zeta_i - \alpha z_s) \cos(k_i s + \omega_i t + \phi_i) - c_1 z_s - c_3 z_s^3 - b_1 \dot{z}_s - b_2 \dot{z}_s^2 \quad (15)$$

The wave component amplitudes  $\zeta_i$ , wave numbers  $k_i$ , and angular frequencies  $\omega_i$  are sampled from a generic wave energy spectrum  $S(\omega)$  given by Eq. (16), where  $H_s$  is the significant wave height and  $\omega_p$  is the peak frequency. The component phase angles  $\phi_i$  are selected randomly from the range  $[-2\pi : 2\pi]$ .

$$S(\omega) = H_s^2 \frac{5}{3} \frac{\omega_p^4}{\omega^5} \exp\left(-\frac{5}{4} \left(\frac{\omega_p}{\omega}\right)^4\right) \quad (16)$$

To cast Eq. (15) in the form of Eq. (14), we must choose a model for  $f^{(l)}(s; t, z_s, \dot{z}_s)$ . This choice will determine the physics that are solved directly versus what must be learned by the ML model for  $\delta_s$ . Five different low-fidelity forcing models are proposed, given by Eqs. (17)-(21), with Eq. (17) having the most physics retained (and consequently the least physics that must be learned in  $\delta_s$ ). In Eq. (21), the entire forcing function must be learned by the ML model.

$$\text{Model A:} \quad f_A^{(l)}(s; t, z_s, \dot{z}_s) = \sum_i \zeta_i \cos(k_i s + \omega_i t + \phi_i) - c_1 z_s - b_1 \dot{z}_s \quad (17)$$

$$\text{B:} \quad f_B^{(l)}(s; t, z_s, \dot{z}_s) = -c_1 z_s - b_1 \dot{z}_s \quad (18)$$

$$\text{C:} \quad f_C^{(l)}(s; t, z_s, \dot{z}_s) = -c_1 z_s \quad (19)$$

$$\text{D:} \quad f_D^{(l)}(s; t, z_s, \dot{z}_s) = \sum_i \zeta_i \cos(k_i s + \omega_i t + \phi_i) - c_1 z_s \quad (20)$$

$$\text{E:} \quad f_E^{(l)}(s; t, z_s, \dot{z}_s) = 0 \quad (21)$$

To further illustrate the differences in the low-fidelity forcing models, Table 1 shows the force contributions that are modeled analytically and those that are data-driven for each choice of forcing model  $f^{(l)}(s; t, z_s, \dot{z}_s)$ .

**Table 1: Forces retained as physics (P) in  $f^{(l)}(s; t, z_s, \dot{z}_s)$  or learned by ML in  $\delta_s$**

		Forcing Model				
Force Description	Term	A	B	C	D	E
Linear Restoring	$c_1 z_s$	<b>P</b>	<b>P</b>	<b>P</b>	<b>P</b>	ML
Nonlinear Restoring	$c_3 z_s^3$	ML	ML	ML	ML	ML
Linear Damping	$b_1 \dot{z}_s$	<b>P</b>	<b>P</b>	ML	ML	ML
Nonlinear Damping	$b_2 \dot{z}_s^2$	ML	ML	ML	ML	ML
Linear Excitation	$\sum_i \zeta_i \cos(\cdot)$	<b>P</b>	ML	ML	<b>P</b>	ML
Nonlinear Excitation	$\sum_i -\alpha z_s \cos(\cdot)$	ML	ML	ML	ML	ML

## RESULTS

The Duffing equation is configured using  $m(s) = 1.0$ ,  $c_1 = 1.0$ ,  $c_3 = 0.01$ ,  $b_1 = 0.1$ ,  $b_2 = \alpha = 0$  so that the only nonlinear term is the cubic restoring force. For a given significant wave height  $H_s$  and peak frequency  $\omega_p$ , the wave elevation  $\eta_s$ , and time series of nonlinear state  $z_s, \dot{z}_s, \ddot{z}_s$  and force correction  $\delta_s$ , are generated by solving Eq. (15) numerically. This is done to generate training data which are used to train the ML model for  $\delta_s$ . In addition, testing data are also generated, but these data are used to verify the performance of the trained models and are not used during the training process, as is discussed later in this section.

Throughout the study, each of the five low-fidelity forcing models given in Table 1 are considered. In all time series, a time step of  $\Delta t = 0.1$  s is used. Also, when sampling the wave spectrum to create  $\eta_s$ , the sample frequency bandwidth is taken

such that the repeat period of the resulting summation is equal to the length of the time series.

An ML model consisting of a feed-forward, densely-connected neural network with 2 hidden layers, 30 nodes per layer, and ReLU activation functions is trained for each  $\delta_s$  corresponding to each low-fidelity forcing model  $f_s^{(l)}$ . In this work, a stencil length  $k = 5$  is used, per the recommendations outlined in Marlantes et al. (2023). The reason a small  $k$  is effective in this case is because the nonlinear force components are functions only of the instantaneous state variables  $z_s$  and  $\dot{z}_s$ . Each model is trained for a total of 1000 epochs until the training loss no longer improves, however, only the weights from the epoch with the lowest loss are retained as final weights. The training time for each model is approximately 1 minute on a modest computing platform.

The average  $L_2$  error,  $L_\infty$  error, given by Eqs. (22) and (23), respectively, are used to evaluate the accuracy of the time series predictions in terms of RMS and extreme values.

$$L_2 = \sqrt{\frac{\sum_i^N (\hat{x} - x)^2}{N}} \quad (22)$$

$$L_\infty = \max(|\hat{x} - x|) \quad (23)$$

However, such measures are sensitive to small phase errors. As a more powerful measure of performance, the Jensen-Shannon divergence (JSD), as given by Eq. (24), is used to estimate the entropy of the predicted response pdf relative to a known reference pdf.  $P$  is the reference distribution and  $Q$  is the model distribution, both being pdfs, and  $M$  is the mixture. The Jensen-Shannon divergence is based on the Kullback-Leibler divergence  $D$ , given by Eq. (25), which is a measure of the relative entropy between the model distribution  $K$  and the reference distribution  $M$ , both defined over the domain  $\chi$ . It can be thought of as a measure of information loss, or expected surprise, if a certain distribution is used to model a reference distribution. A lower JSD means the model is closer to the reference, with a divergence of zero meaning the two distributions are identical.

$$JSD(P\|Q) = \frac{1}{2}D(P\|M) + \frac{1}{2}D(Q\|M) \quad (24)$$

$$M = \frac{1}{2}(P + Q)$$

$$D(K\|M) = \sum_{x \in \chi} K(x) \log \left( \frac{K(x)}{M(x)} \right) \quad (25)$$

The  $L_2$ ,  $L_\infty$ , and JSD metrics will be evaluated on predictions of the sectional acceleration  $\ddot{z}_s$  as it captures both the accuracy of the force integral on the right-hand-side of Eq. (9), as well as the inertial force of the entire beam to a constant factor.

## Training Data Size

We wish to use the smallest training dataset possible, so the influence of training dataset size on prediction accuracy is first investigated. Using a significant wave height  $H_s = 1.0$  and a peak frequency of  $\omega_p = 1.0$ , irregular wave records of  $\eta_s$  ranging in total length of 10 s up to 1000 s are generated, and the corresponding responses  $z_s$ ,  $\dot{z}_s$ ,  $\ddot{z}_s$ , and the force correction  $\delta_s$  are computed. Using this data, an ML model is trained for each low-fidelity forcing model in Table 1. The trained models are used to make predictions of the response in 1000 s of irregular waves with the same  $H_s = 1.0$  and  $\omega_p = 1.0$ , but with different random phase angles. For each model, the  $L_2$ ,  $L_\infty$ , and JSD are computed. Figure 2 shows the prediction errors vs

training dataset size for each low-fidelity forcing model. Note that the training dataset size is given as the number of Zero-Up-Crossings (ZUCs) in the wave record, as this is a more meaningful measure of response encounters than time alone.

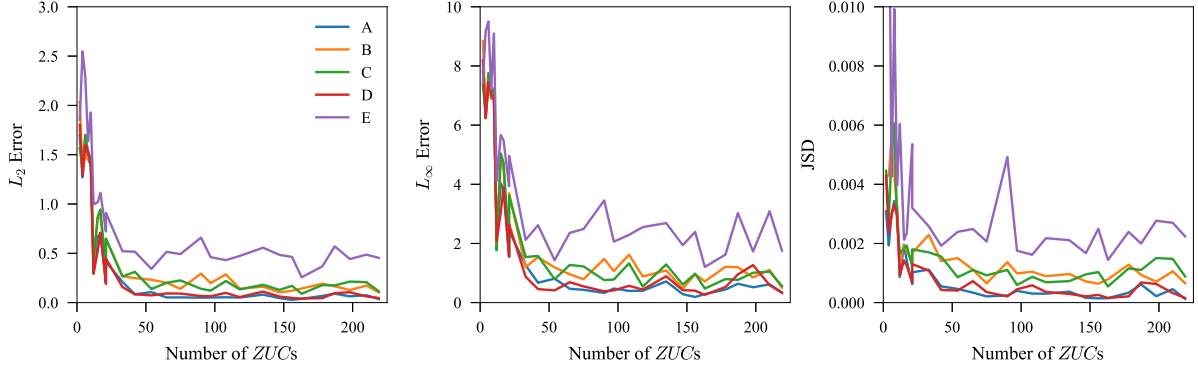


**Figure 2:**  $L_2$ ,  $L_\infty$ , and  $JSD$  prediction errors for each low-fidelity forcing model over increasing training data size measured in wave record Zero-Up-Crossings (ZUCs). Predictions are in irregular waves  $H_s = 1.0$ ,  $\omega_p = 1.0$ , with random phase angles that differ from the training dataset.

Figure 2 shows that prediction errors of the five different models converge at roughly the same rate relative to the size of the training dataset. Datasets of approximately 50 ZUCs and larger yield similar prediction errors, with the exception of model E, which requires at least 100 ZUCs.

### Generalizability in $H_s$

Training data is generated for two different significant wave heights,  $H_s = 0.7$  and  $H_s = 1.0$ , at a peak frequency of  $\omega_p = 1.0$  for a total time series length of 500 s, or about 108 ZUCs to correspond with the findings in Figure 2. The time series for the state variables  $z_s$ ,  $\dot{z}_s$ ,  $\ddot{z}_s$ , and wave elevation  $\eta_s$  are shown in Figure 3.

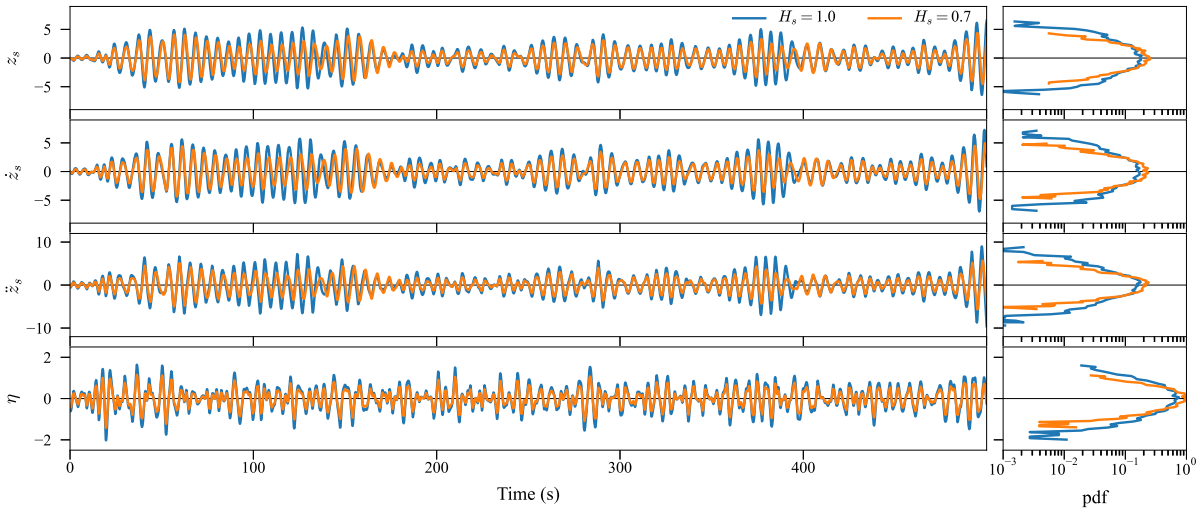


**Figure 3:** Training data time series for Duffing equation:  $m(s) = 1.0$ ,  $c_1 = 1.0$ ,  $c_3 = 0.01$ ,  $b_1 = 0.1$ ,  $b_2 = \alpha = 0$ , in irregular waves:  $H_s = 0.7$  and  $H_s = 1.0$ ,  $\omega_p = 1.0$ .

Figure 4 shows the corresponding  $\delta_s$  for each low-fidelity forcing model for the training data case  $H_s = 1.0$  and  $\omega_p = 1.0$ . Note the difference in magnitude of  $\delta_s$  between the models, where  $\delta_{E,s}$  encompasses all of the hydrodynamic forces.

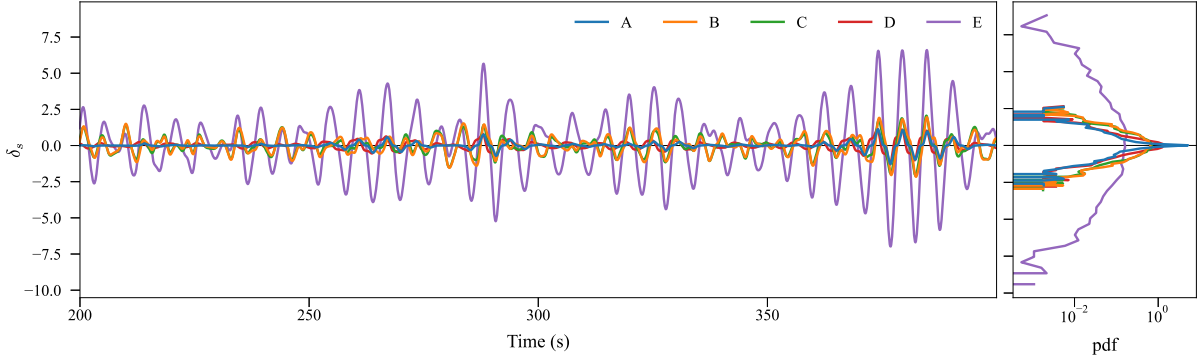
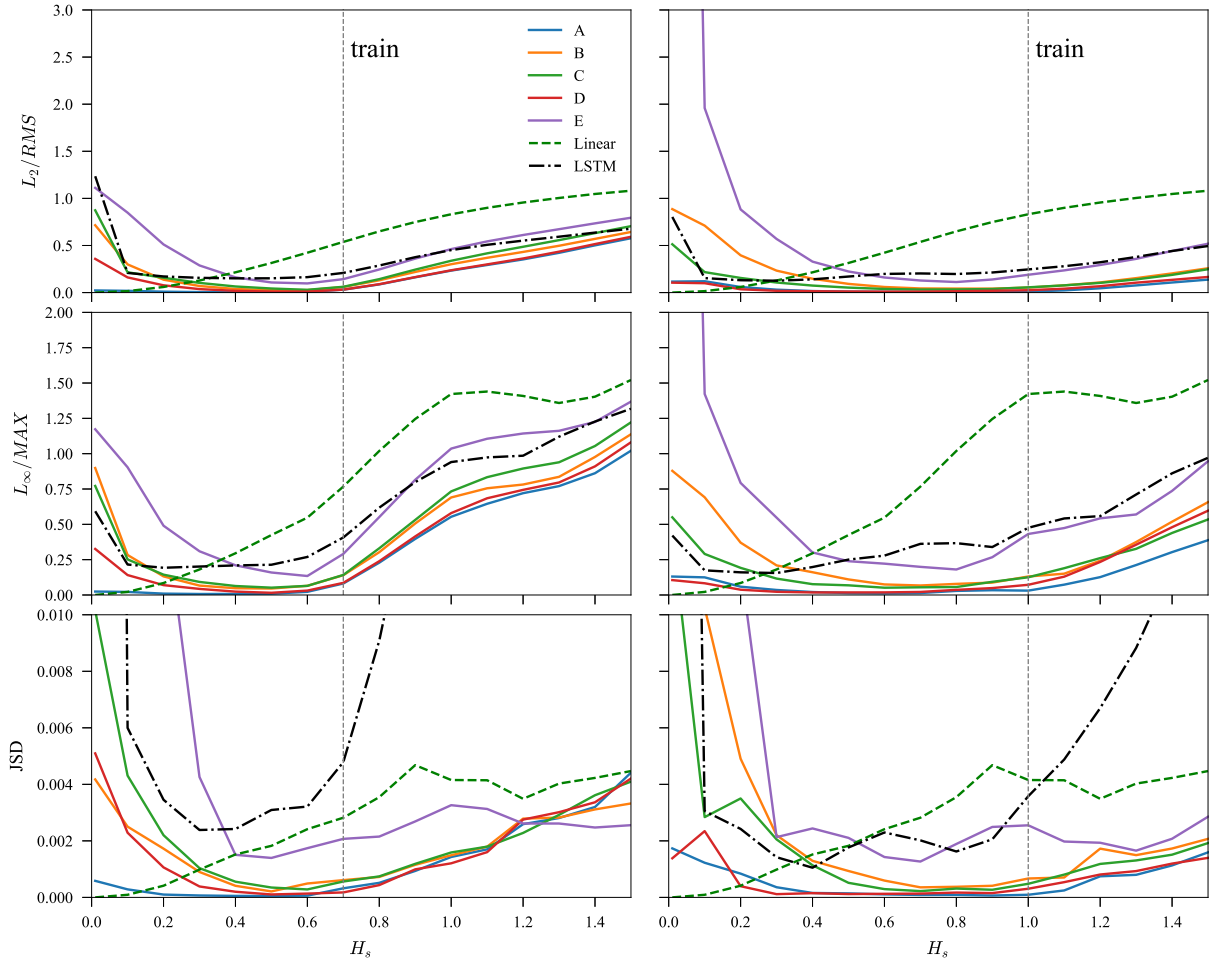


**Figure 4: Training data for force correction  $\delta_s$  for the five different low-fidelity forcing models  $f_j^{(l)}$ ,  $j = A, B, C, D, E$  in irregular waves:  $H_s = 1.0$ ,  $\omega_p = 1.0$ . The time series is given only from 200 s to 400 s so that the difference between the models is easier to distinguish, however, the pdfs are generated from the entire 500 s time series.**

Training data for two different  $H_s$  are shown in Figure 3, however, only one realization will be used for training at one time. This represents the minimum useful training dataset: 100 ZUCs in a single  $H_s$ . ML models for each of the five low-fidelity forcing models are trained at each wave height, to investigate any difference the training  $H_s$  may have on the performance of the models when making predictions.

As a benchmark, a Long Short-Term Memory (LSTM) neural network is also trained using a sequence-to-sequence paradigm, where the entire wave elevation  $\eta_s$  is used as the input to the network, and the output is the corresponding responses  $z_s$ ,  $\dot{z}_s$ , and  $\ddot{z}_s$ . LSTM networks and their variants are widely used in literature on data-driven modeling of marine dynamics (Xu et al., 2021), (Silva and Maki, 2022), and may be the predominant data-driven model for time series modeling. Due to its popularity, the LSTM is chosen for comparison. The network is composed of 4 hidden layers with 50 cells per layer to mimic the models used in Xu (2020). The model is trained for 200 epochs, until the loss plateaus at a value less than 1%. The best weights during the training process are restored at the end of the training process. The training time for the LSTM network using the data in Figure 3 is approximately 2 hours on a modest computing platform.

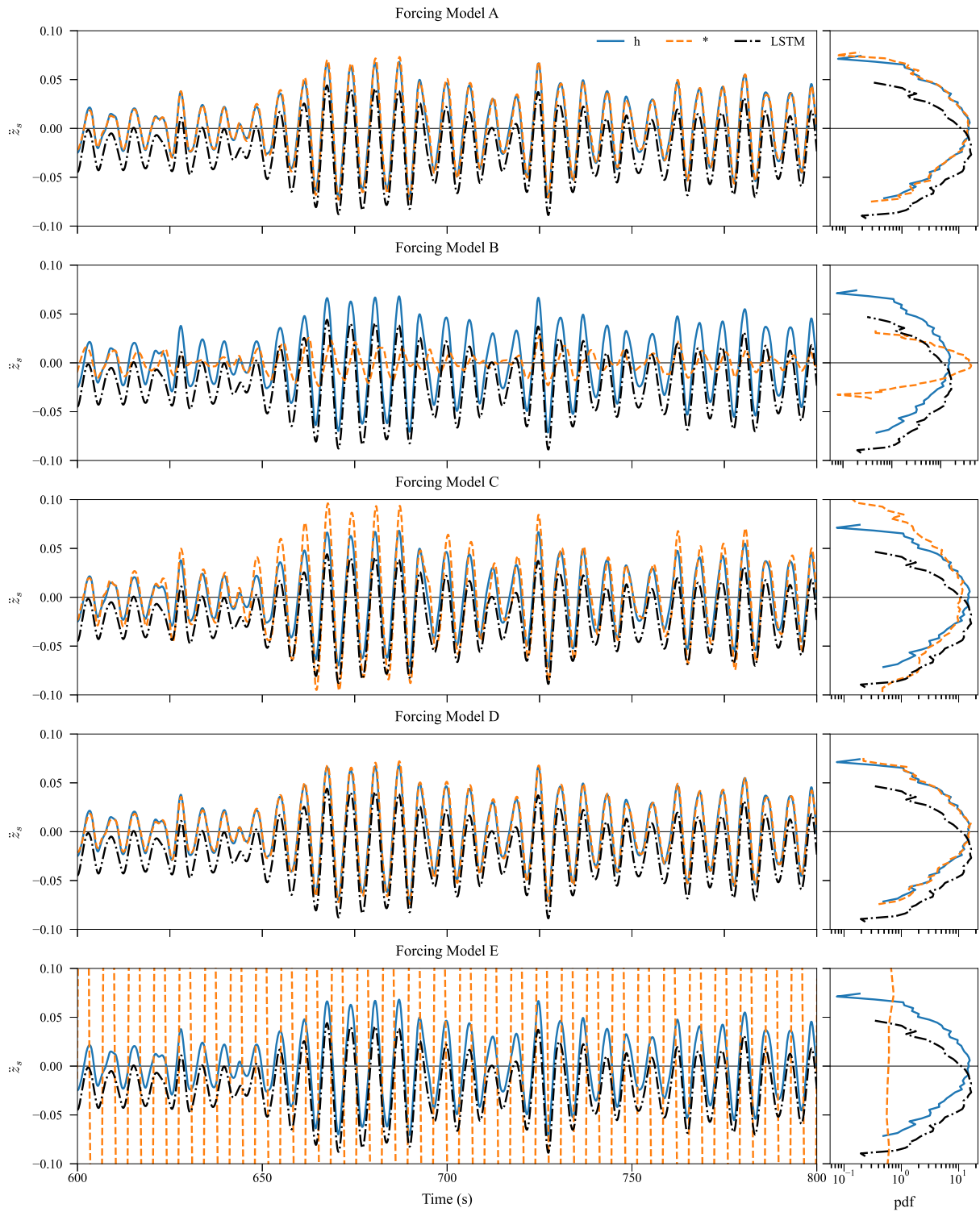
A testing dataset is generated for a range of significant wave heights  $H_s$  from 0.01 to 1.5 and a peak frequency  $\omega_p = 1.0$  over 1000 s of time. The component phase angles  $\phi_i$  are selected randomly to differ from the phase angles used in the training dataset. Each trained ML model is used to make predictions of the responses in each  $H_s$  from the testing dataset. Using Eqs. (22) through (24), the  $L_2$ ,  $L_\infty$ , and JSD metrics for the predictions are computed over the last 900 s of time series, omitting the first 100 s as it is a transient region. Figure 5 shows the performance metrics for each low-fidelity forcing model, the LSTM predictions, and a benchmark linear model, over the range of test significant wave heights. The wave height that was used for training is marked by a vertical line in each figure.



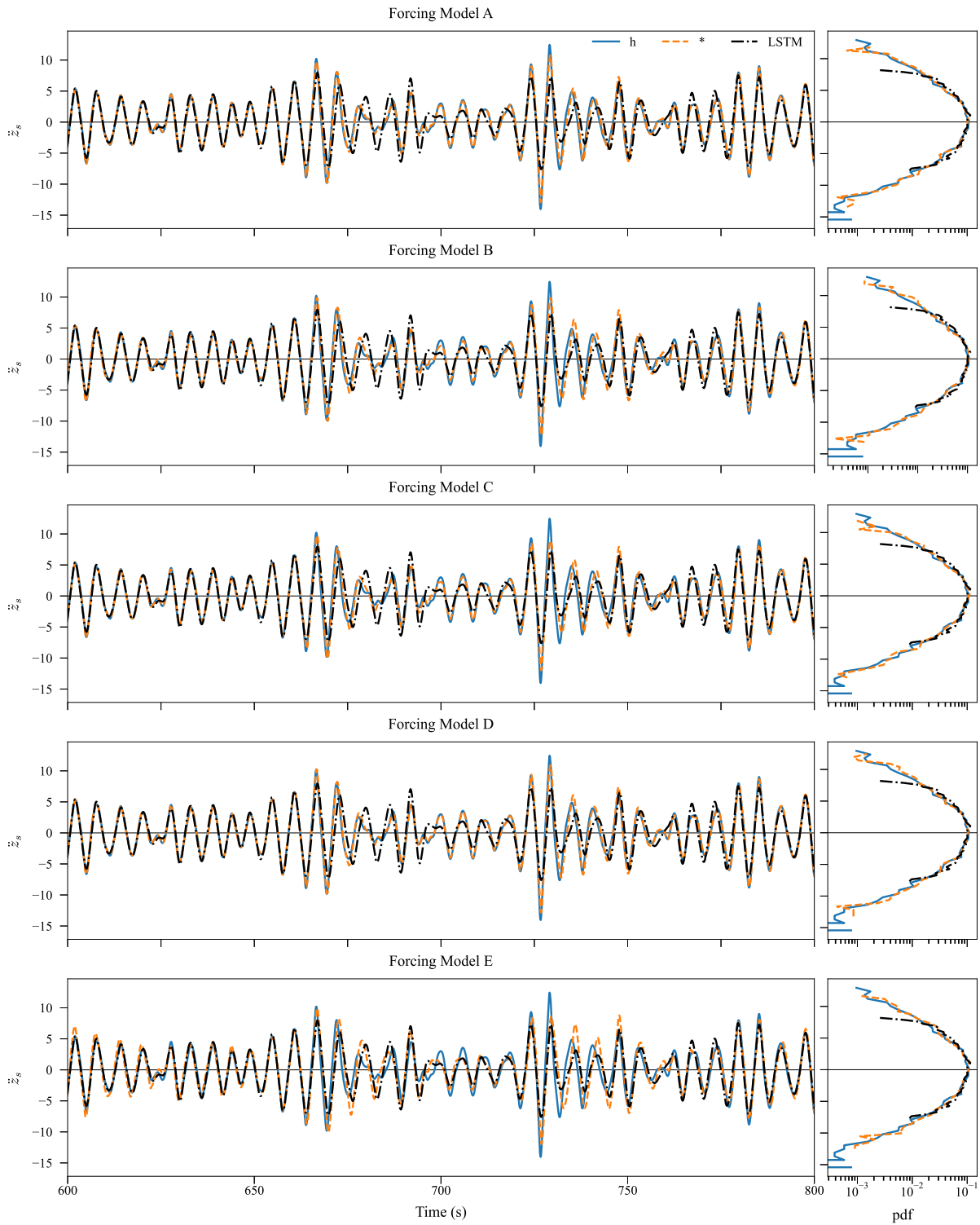
**Figure 5:**  $L_2$ ,  $L_\infty$ , and JSD error metrics for predictions of  $\ddot{z}_s$  for different low-fidelity forcing models over a range of  $H_s$ . The left panels correspond to models trained using  $H_s = 0.7$ , and the right panels  $H_s = 1.0$ . Results from the LSTM predictions are also shown for comparison. The linear model is also included to show how the linear error decreases to zero in the limit of small significant wave heights.

Figure 5 shows model A—the model that retains the most physics—performs better than the other models, and the LSTM benchmark, in nearly all wave conditions. This suggests that the more physics that are retained as analytical terms in the model, i.e. not data-driven, the generalizability of the model is improved. This is especially evident at low wave heights, where the low-fidelity physics enforce the correct dynamics at the linear limit. The  $L_2$  and  $L_\infty$  errors from the LSTM predictions are roughly in line with model E, which is perhaps intuitive as it is almost a purely data-driven model as well. Training in larger  $H_s$  seems to reduce prediction errors in larger  $H_s$ , while slightly increasing prediction errors at low- $H_s$ . However, this difference is greatly reduced in models which retain more physics.

To emphasize the performance of model A further, Figures 6 and 7 give the time series and pdfs of the predictions for each forcing model and the LSTM benchmark at the smallest  $H_s = 0.01$  and the largest  $H_s = 1.5$  significant wave heights. It is shown that the LSTM model struggles in both extremes, especially to predict the tails of the distribution. In comparison, models A and D perform well for both cases. Model E performs the worst, greatly over-predicting the response in small  $H_s$ , appearing as rapid, but stable, oscillations. Consider the pdf for model A at  $H_s = 0.01$  in Figure 6 and note the sensitivity of the JSD to small errors in the predicted distributions, as this proposed model fits qualitatively well to the reference distribution, but the small errors in the tails are magnified in Figure 5.



**Figure 6: Predictions of  $\ddot{z}_s$  in irregular waves  $H_s = 0.01$ ,  $\omega_p = 1.0$  using the proposed method with different low-fidelity forcing models. Each model is trained in irregular waves with  $H_s = 1.0$ ,  $\omega_p = 1.0$ . Results from an LSTM prediction are also shown for comparison. Only 200 s of response is shown for clarity, however, the distributions encompass the entire 1000 s time series.**



**Figure 7: Predictions of  $\ddot{z}_s$  in irregular waves  $H_s = 1.5$ ,  $\omega_p = 1.0$  using the proposed method with different low-fidelity forcing models. Each model is trained in irregular waves:  $H_s = 1.0$ ,  $\omega_p = 1.0$ . Results from an LSTM prediction are also shown for comparison. Only 200 s of response is shown for clarity, however, the distributions encompass the entire 1000 s time series.**

## CONCLUSIONS

The results of this study show that the neural-corrector method of Marlantes and Maki (2022) can be extended to the global loads problem and provide predictions in a range of irregular wave conditions that differ from the original training dataset. It is also found that retaining low-fidelity physics greatly improves the generalizability of the model. The accuracy of the predictions exceeds that of an LSTM benchmark when trained on an equivalent training dataset, especially in preserving the tails of the response distributions. The fact that a simple, feed-forward neural network as used in the proposed method offers improved performance over a typical LSTM model is largely due to the inclusion of low-fidelity physics in the formulation. A well-tuned linear model intrinsically captures much of the important dynamics of the problem, so that the ML correction must learn only higher-order terms, as shown in Marlantes and Maki (2022), such that a much simpler network is adequate. Finally, the proposed method, when including the most physics in the low-fidelity forcing model, requires a dataset of responses encompassing only 50 - 100 irregular wave encounters.

This work considered the responses of only a single section of the global loads problem. To implement multiple sections in unison, there are two possibilities: training a single model with multiple output nodes corresponding to a spatial discretization of  $\delta(x; t, z, \dot{z})$  at different longitudinal locations; or, training multiple models with single node outputs—such as done in this paper. In the former case, the output nodes must respect the integral on the right-hand-side of Eq. (9), which could be enforced in the loss function during training.

## CONTRIBUTION STATEMENT

**Kyle E. Marlantes:** Conceptualization; data curation; formal analysis; software; visualization; methodology; writing – original draft. **Kevin J. Maki:** Conceptualization; supervision; methodology; writing – review and editing.

## ACKNOWLEDGEMENTS

This work was supported financially by grants from the US Office of Naval Research (ONR).

## REFERENCES

- Alford, L. K. (2008). *Estimating Extreme Responses Using a Non-Uniform Phase Distribution*. PhD thesis.
- Alford, L. K., Kim, D.-H., and Troesch, A. W. (2011). Estimation of extreme slamming pressures using the non-uniform fourier phase distributions of a design loads generator. *Ocean Engineering*, 38(5):748–762.
- Anastopoulos, P. A. and Spyrou, K. J. (2016). Ship dynamic stability assessment based on realistic wave group excitations. *Ocean Engineering*, 120:256–263.
- Andersen, I. M. V. and Jensen, J. J. (2014). Measurements in a container ship of wave-induced hull girder stresses in excess of design values. *Marine Structures*, 37:54–85.
- Gaspar, B., Teixeira, A., and Guedes Soares, C. (2016). Effect of the nonlinear vertical wave-induced bending moments on the ship hull girder reliability. *Ocean Engineering*, 119:193–207.
- Guedes Soares, C. (1991). Effect of transfer function uncertainty on short-term ship responses. *Ocean Engineering*, 18(4):329–362.

- Hirdaris, S., Bai, W., Dessi, D., Ergin, A., Gu, X., Hermundstad, O., Huijsmans, R., Iijima, K., Nielsen, U., Parunov, J., Fonseca, N., Papanikolaou, A., Argyriadis, K., and Incecik, A. (2014). Loads for use in the design of ships and offshore structures. *Ocean Engineering*, 78:131–174.
- Hou, C., Wang, W., Li, Y., Wang, X., Zhang, H., and Hu, Z. (2024). A predicting method for the mechanical property response of the marine riser based on the simulation and data-driven models. *Ocean Engineering*, 293:116612.
- Juncher, J. and Terndrup, P. (1979). Wave induced bending moments in ships—a quadratic theory.
- Kwon, D.-S., Jin, C., and Kim, M. (2022). Prediction of dynamic and structural responses of submerged floating tunnel using artificial neural network and minimum sensors. *Ocean Engineering*, 244:110402.
- Marlantes, K. E., Bandyk, P. J., and Maki, K. J. (2023). Investigating nonlinear forces in ship dynamics using machine learning. In *Proceedings of the 10th International Conference on Computational Methods in Marine Engineering (MA-RINE)*, Madrid, Spain.
- Marlantes, K. E. and Maki, K. J. (2022). A neural-corrector method for prediction of the vertical motions of a high-speed craft. *Ocean Engineering*, 262:112300.
- Marlantes, K. E. and Taravella, B. M. (2019). A fully-coupled quadratic strip theory/finite element method for predicting global ship structure response in head seas. *Ocean Engineering*, 187:106189.
- Moreira, L. and Soares, C. G. (2020). Neural network model for estimation of hull bending moment and shear force of ships in waves. *Ocean Engineering*, 206:107347.
- Parunov, J., Guedes Soares, C., Hirdaris, S., Iijima, K., Wang, X., Brizzolara, S., Qiu, W., Mikulić, A., Wang, S., and Abdelwahab, H. (2022a). Benchmark study of global linear wave loads on a container ship with forward speed. *Marine Structures*, 84:103162.
- Parunov, J., Guedes Soares, C., Hirdaris, S., and Wang, X. (2022b). Uncertainties in modelling the low-frequency wave-induced global loads in ships. *Marine Structures*, 86:103307.
- Payer, H. G. and Schellin, T. E. (2013). A class society's view on rationally based ship structural design. *Ships and Offshore Structures*, 8(3-4):319–336.
- Portillo Juan, N. and Negro Valdecantos, V. (2022). Review of the application of artificial neural networks in ocean engineering. *Ocean Engineering*, 259:111947.
- Rajendran, S., Fonseca, N., and Soares, C. G. (2016). Prediction of extreme motions and vertical bending moments on a cruise ship and comparison with experimental data. *Ocean Engineering*, 127:368–386.
- Schellin, T. E., Shigunov, V., Troesch, A. W., Kim, D.-H., and Maki, K. (2015). Prediction of loads for ship structural design. *Naval Engineers Journal*, 127(1):103–134.
- Silva, K. M. and Maki, K. J. (2022). Data-driven system identification of 6-dof ship motion in waves with neural networks. *Applied Ocean Research*, 125:103222.
- Temarel, P., Bai, W., Bruns, A., Derbanne, Q., Dessi, D., Dhavalikar, S., Fonseca, N., Fukasawa, T., Gu, X., Nestegård, A., Papanikolaou, A., Parunov, J., Song, K., and Wang, S. (2016). Prediction of wave-induced loads on ships: Progress and challenges. *Ocean Engineering*, 119:274–308.
- Wang, H. and Ti, Z. (2024). Wave force prediction on truncated cylinders with arbitrary symmetric cross-sections using machine learning. *Ocean Engineering*, page 116716.
- Willard, J., Jia, X., Xu, S., Steinbach, M., and Kumar, V. (2020). Integrating physics-based modeling with machine learning: A survey.
- Wu, M. and Hermundstad, O. A. (2002). Time-domain simulation of wave-induced nonlinear motions and loads and its applications in ship design. *Marine Structures*, 15(6):561–597.

- Xu, W. (2020). *A Machine Learning Framework to Model Extreme Events for Nonlinear Marine Dynamics*. PhD thesis, University of Michigan, Ann Arbor, MI.
- Xu, W., Maki, K. J., and Silva, K. M. (2021). A data-driven model for nonlinear marine dynamics. *Ocean Engineering*, 236:109469.
- Zhu, J. and Collette, M. (2017). A bayesian approach for shipboard lifetime wave load spectrum updating. *Structure and Infrastructure Engineering*, 13(2):298–312.